Preprints.org

Article

Not peer-reviewed version

Proposal of the FPGA Neural Network Trigger for a Recognition of Chemical Composition of the Ultra High-Energy Cosmic Rays in the Pierre Auger Surface Detector

Zbigniew Szadkowski * and Krzysztof Pytel

Posted Date: 5 March 2026

doi: 10.20944/preprints202603.0364.v1

Keywords: neural network; trigger; FPGA; water Cherenkov detectors

Preprints.org is a free multidisciplinary platform providing preprint service that is dedicated to making early versions of research outputs permanently available and citable. Preprints posted at Preprints.org appear in Web of Science, Crossref, Google Scholar, Scilit, Europe PMC.

Copyright: This open access article is published under a Creative Commons CC BY 4.0 license, which permit the free download, distribution, and reuse, provided that the author and preprint are cited in any reuse.

Preprints.org (www.preprints.org) | NOT PEER-REVIEWED | Posted: 5 March 2026 doi:10.20944/preprints202603.0364.v1

Disclaimer/Publisher's Note: The statements, opinions, and data contained in all publications are solely those of the individual author(s) and contributor(s) and not of MDPI and/or the editor(s). MDPI and/or the editor(s) disclaim responsibility for any injury to people or property resulting from any ideas, methods, instructions, or products referred to in the content.

Article

Proposal of the FPGA Neural Network Trigger for a Recognition of Chemical Composition of the Ultra High-Energy Cosmic Rays in the Pierre Auger Surface Detector

Zbigniew Szadkowski [1,*] and Krzysztof Pytel [2]

[1] University of Łódź, Faculty of Physics and Applied Informatics, Department of Intelligent Systems, 90-236 Łódź, Pomorska 149, Poland
[2] University of Łódź, Faculty of Physics and Applied Informatics, Department of Informatics, 90-236 Łódź, Pomorska 149, Poland
* Correspondence: zbigniew.szadkowski@uni.lodz.pl; Tel.: +48-42-635-56-59

Abstract

The standard first-level trigger in the Pierre Auger Observatory surface detectors (data analysis in FPGAs immediately after digitization in ADCs) were developed when FPGAs were relatively simple and additionally expensive. Thus algorithms developed in 90's of the previous century are relatively simple. Huge progress in electronics allows the implementation of very sophisticated mathematical algorithms in very efficient systems and relatively inexpensive FPGAs. A neural network is an alternative trigger developed recently for recognition neutrino-induced showers gave relatively high efficiency and allowed distinguishing signal profiles from Auger photo-multiplier tubes of water-Cherenkov detectors originating from atmospheric showers induced by high-background neutrinos from other showers. The chemical composition of ultra high-energy cosmic rays (UHECR) is sophisticated and still not known. Additional tool analyzing online in real time a potential chemical composition could help fix this problem.

Keywords: neural network; trigger; FPGA; water Cherenkov detectors

1. Introduction

The origin of ultra-high-energy cosmic rays (UHECR) is still a mystery [1–5]. Anisotropy, mass composition and the energy spectrum are the fundamental topics investigating the nature of the ultra-high energy cosmic rays. Extremely low UHECR stream (estimated from a single super-energetic particle per km^2 and age) requires very large ground-based experiments spread on thousands of km^2, like the Pierre Auger Observatory [6].

The suppression of the flux is observed above 40 EeV [7,8]. This suggests that the energy of the UHECRs is attenuated by interactions with the cosmic microwave background and infrared photons on their journey from their extra-galactic sources (inverse Compton effect), either by photo-pion interactions in the case of protons or by photo-disintegration in the case of nuclei [9,10] (Greisen-Zatsepin-Kuzmin effect known as GZK). In consequence the sources of highest energies cosmic rays can be located within the so-called GZK horizon (which is e.g. ∼200 Mpc for protons above 60 EeV [11,12]). The Pierre Auger Collaboration [13–15] reports the correlation between the arrival directions of cosmic rays with energies above 55 EeV and the distribution of nearby extra-galactic objects.

Consider a scenario where several nuclear components contribute to the total intensity, where the nuclei are accelerated to a maximum energy proportional to their electric charge (Z). This scenario, e.g. [16–19], explains the trend towards heavier masses with increasing energy [20–22]. We assume here, several nuclear components injected into the sources, where the power-law spectrum and the maximum energy of the sources are modeled with an exponential cut-off without too much detail.

© 2026 by the author(s). Distributed under a Creative Commons CC BY license.

Preprints.org (www.preprints.org) | NOT PEER-REVIEWED | Posted: 5 March 2026 doi:10.20944/preprints202603.0364.v1

Figure 1 shows the best reproduction of the data by simultaneously fitting the energy spectrum above 5 EeV and the depth distribution of the cascade maximum (Xmax), which is sensitive to mass (using the LHC EPOS [23] as a model of hadronic interactions in their interpretation). The nuclear element count in the sources is dominated by intermediate-mass nuclei accelerated to ∼5*Z EeV and escaping from the source environments with a very hard spectrum. In this scenario, the observed steep slope above ∼50 EeV results from the combination of the maximum acceleration energy of the heaviest nuclei in the sources and the GZK effect. The steepness at ∼ 10 EeV reflects the interaction between the contributions of the helium flux and the CNO components injected into the source with their distinct cut-off energies, shaped by photo-disintegration during propagation.

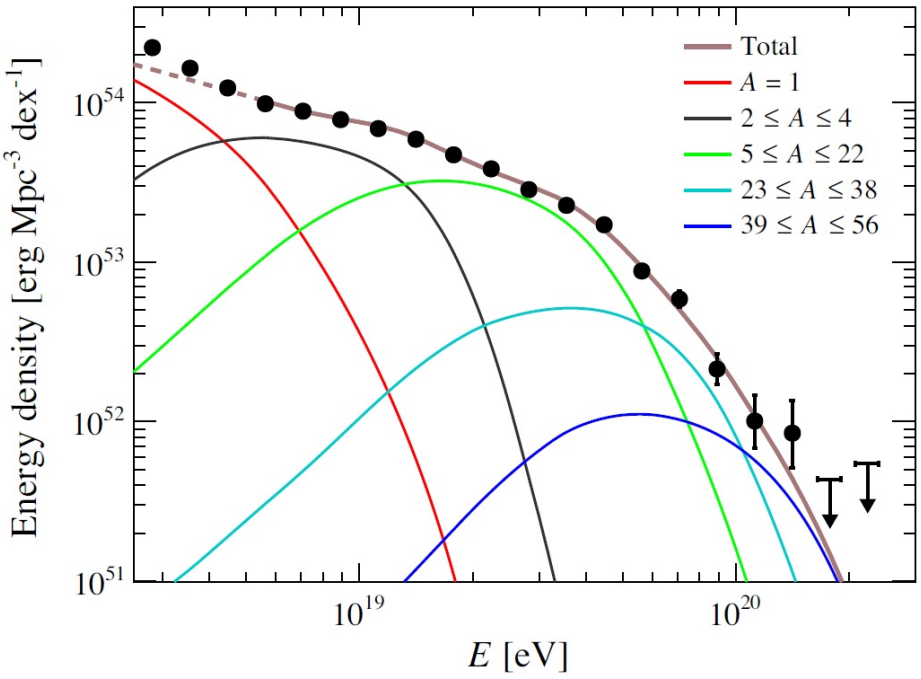

Figure 1. Energy density obtained with the best fit parameters of the benchmark scenario used for illustration, as described in the text. The dashed curve shows the energy range that is not used in the fit and where an additional component is needed for describing the spectrum [24]. For simplicity, the sources are assumed to be stationary and homogeneous in the co-moving volume.

Figure 1 informs that the chemical composition of UHECR is complicated and a lot of heavy ions may appear in cosmic ray stream. Verification of assumed models requires detailed simulation of a development of Extensive Air Showers (EAS) in the atmosphere by CORSIKA (COsmic Ray Simulations for KAscade) package [25] and in the surface detector (OffLine package [26]).

Figure 2 shows experimental data from various experiments related to the various hadron models of interactions (Sibyll 2.3d, QGSjet-II.04 and EPOS-LHC). It is explicitly shown that the contribution of heavy ions is not negligible.

Our previous analysis trying to recognize initial particles from neutrino or other one [27] gave a very promising results distinguishing neutrinos from protons at a level of 97% (Table 1).

Table 1. The recognition efficiency (in %) of neutrinos and others particles, respectively, for THR=100 ADC_units and for various thresholds for the 8-6-1 architecture of the neural network.

ver	ν	others	ν	others
THR	0.0	0.0	0.5	-0.5
%	98.63	97.35	97.39	96.2

We continue our approach simulating also a development of showers initiating by helium, carbon, nitrogen, oxygen and iron heavy ions.

© 2026 by the author(s). Distributed under a Creative Commons CC BY license.

Preprints.org (www.preprints.org) | NOT PEER-REVIEWED | Posted: 5 March 2026 doi:10.20944/preprints202603.0364.v1

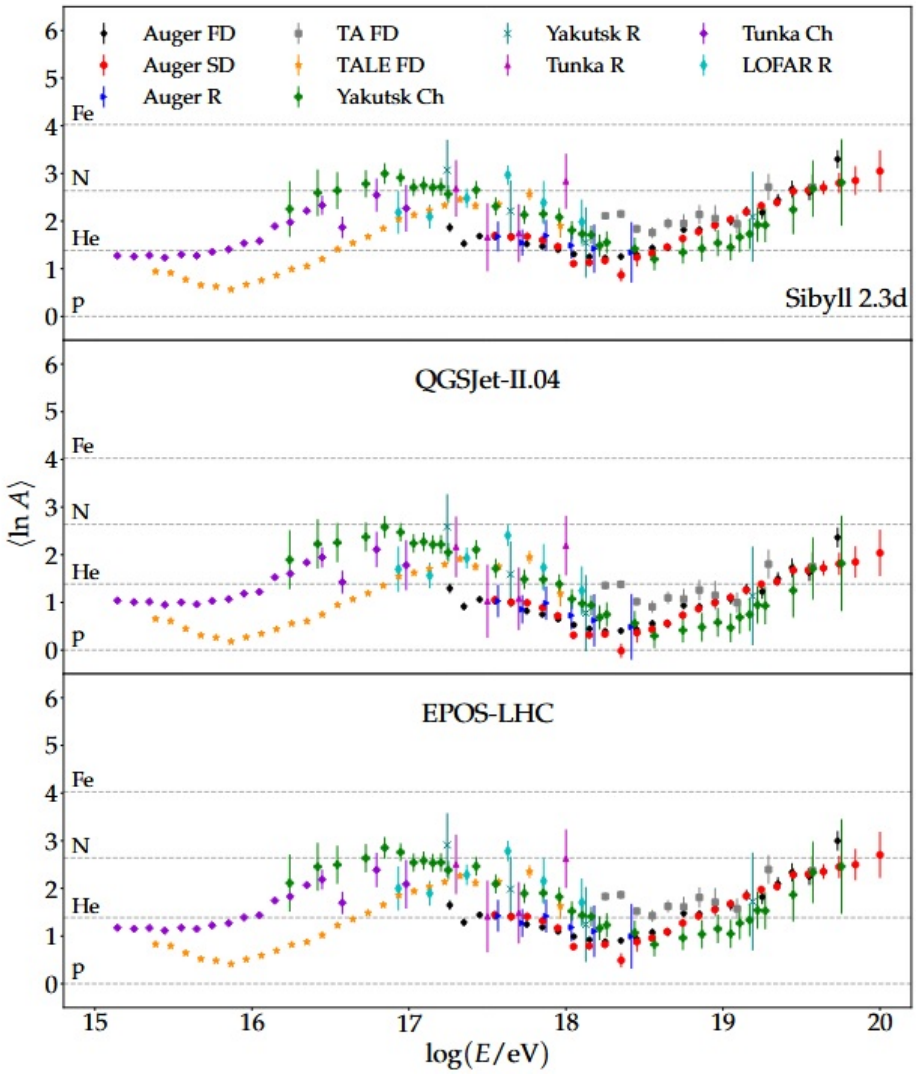

Figure 2. Mean value of ln A as a function of the logarithmic energy obtained from ⟨Xmax⟩ measured by different experiments. Three different high-energy hadronic interaction models are used to interpret the data [28].

2. Input Data

We ran simulations for zenith angles: 70°, 75°, 80°, 85°, 89° and the energies of primary particles: $3*10^8$, 10^9, $3*10^9$ and 10^{10} GeV for protons and muon neutrinos, helium, carbon, nitrogen, oxygen and iron heavy ions in CORSIKA and OffLine packages.

CORSIKA is a program for detailed simulation of extensive air showers initiated by high energy cosmic ray particles. Protons, light nuclei up to iron, photons, and many other particles may be treated as primaries. The particles are tracked through the atmosphere until they undergo reactions with the air nuclei or - in the case of unstable secondaries - decay. The hadronic interactions at high energies may be described by five reaction models alternatively: The VENUS, QGSJET, and DPMJET models are based on the Gribov-Regge theory, while SIBYLL is a minijet model. HDPM is a phenomenological generator and adjusted to experimental data wherever possible. Hadronic interactions at lower energies are described either by the more sophisticated GHEISHA interaction routines or the rather simple ISOBAR model. In particle decays all decay branches down to the 1 % level are taken into account. For electromagnetic interactions the shower program EGS4 or the analytical NKG formulas may be used. Options for the generation of Cherenkov radiation and neutrinos exist.

The Offline software framework of the Pierre Auger Observatory provides an infrastructure to support construction of the various applications necessary to analyze data gathered by the observatory. Specifically, the Offline software supports simulation and reconstruction of events using surface,

© 2026 by the author(s). Distributed under a Creative Commons CC BY license.

Preprints.org (www.preprints.org) | NOT PEER-REVIEWED | Posted: 5 March 2026 doi:10.20944/preprints202603.0364.v1

fluorescence and hybrid methods, as well as simulation of calibration techniques [2] and other ancillary tasks such as data pre-processing. We used this part responsible for calculation of the photo-multipliers response on the Cherenkov light in the surface detectors.

The first interaction of neutrinos usually is deeply into the Earth's atmosphere, due to a very small cross-section for interactions. A cross-sections of protons and heavy ions are much larger than neutrinos, so they usually interact very early entering the Earth's atmosphere. For showers starting their development at the beginning of the Earth's atmosphere, the hadron and electromagnetic components vanish and only the muon component survives at the detector level.

ADC profiles as results of simulations give a very wide spectrum of amplitude and time dispersion. Strong signals with amplitude bigger than 1.75 VEM in all three channels can be detected by the standard Auger trigger and there is no need to be analyzed them by some other trigger. These profiles were neglected in our analysis. The standard single bin trigger in the UB (Unified Boards - for 40 MHz sampling) was three-fold coincidence in a single time bin. For the UUB (Updated Unified Board - 120 MHz sampling) the acceptance window seems to be too narrow and it has been enlarged to three consecutive windows.

3. ANN Models for Classifying Cosmic Ray Particles

An artificial neural network (ANN) is used to analyze the chemical composition and classify cosmic ray particles. Due to the limitations of FPGAs in terms of computational resources, energy consumption, and computation time, the proposed neural network must remain relatively simple. Several feedforward neural network models were selected for analysis. Modeling and testing of the networks were performed in MATLAB using the Neural Network Toolbox.

Model 1 is a three- to six-layer feedforwardnet with five neurons in the output layer. Each neuron in the output layer corresponds to a specific particle type, for example, neuron 1 for neutrino, neuron 2 for proton, neuron 3 for helium, neuron 4 for CNO, and neuron 5 for iron. A diagram of this network is shown in Figure 3. The best results from five training cycles of the network are presented in Table 2.

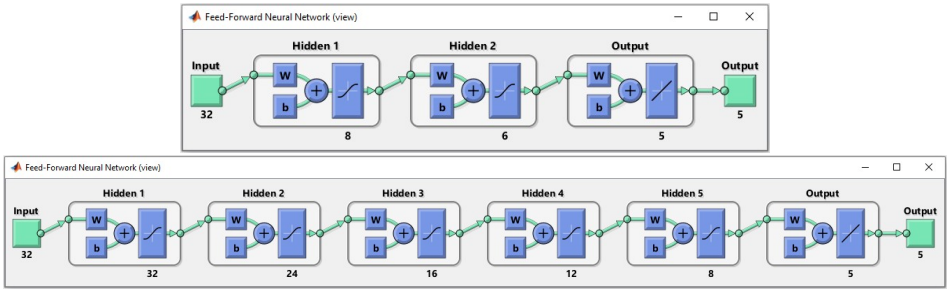

Figure 3. Diagrams of ANN networks: the simplest 8-6-5 and the most complicated 32-24-16-12-8-5.

Table 2. The recognition efficiency (in %) of neutrinos, protons, He, CNO and iron ions respectively, for THR=100 ADC_units, for 3-fold extended coincidences from sub-triggers from 3 channels for various architectures of the neural network, for 32 input time-bins with the maximum on the 10^{th} position, as in the previous (neutrino vs. others) analysis [27].

architecture	8-6-5	12-8-5	20-12-8-5	24-16-12-8-5	32-24-16-12-8-5
neutrino	77.0	84.0	80.2	80.4	79.0
proton	88.7	90.2	88.9	88.4	91.3
He	1.84	0.8	3.0	0.94	1.8
CNO	13.8	23.8	23.9	21.6	22.3
Fe	17.1	11.4	14.1	11.4	19.8

Results from Table 2 are unsatisfactory, especially for helium ions. On the other hand, neutrinos are recognized on a pretty good level. We applied much more complicated even sophisticated neural

© 2026 by the author(s). Distributed under a Creative Commons CC BY license.

Preprints.org (www.preprints.org) | NOT PEER-REVIEWED | Posted: 5 March 2026 doi:10.20944/preprints202603.0364.v1

network 32-24-16-12-8-5 (instead of 8-6-5) expecting better efficiency. Input data are from 32 time-bins, while the maximum of the profile has been established for the 10^{th} index.

Results even for very complicated network are very similar to the relatively simple network. In all architectures protons and neutrinos are recognized pretty good, however, the recognition efficiency for other particles is much lower, for helium is fatal.

Table 3 shows that the new neural network improved only a little bit the previous results. We checked also the maximum position on the 16^{th} index.

Table 3. The recognition efficiency (in %) of neutrinos, protons, He, CNO and iron ions respectively, for THR=100 ADC_units, for 3-fold extended coincidences from sub-triggers from 3 channels for 12-8-5 architecture of the neural network, for 32 input time-bins with the maximum on the 16^{th} position.

particle	1 (%)	2 (%)	3 (%)	4 (%)	5 (%)	avr (%)
neutrino	80.3	80.7	84.2	82.4	81.9	81.9
proton	92.5	90.3	91.3	92.4	91.8	91.85
He	0.75	1.5	1.94	1.16	1.3	1.3
CNO	19.7	22.0	20.7	19.9	20.3	20.3
Fe	22.6	17.4	13.3	18.9	18.6	18.6

As you can see, neutrinos and protons are recognized at a quite satisfactory level. We considered a cascade model recognizing neutrinos, protons and the rest of particles in the first step, and He, CNO, Fe in the second one.

In Model 2, particle recognition is performed using a two-step cascade. The ANN has three neurons in the output layer. In the first step, the outputs correspond to neutrinos, protons, and background signals. If the result of this step indicates "background" (assumed to mean an unidentified or ambiguous particle), the second step is triggered. In this step, the network determines whether the particle is helium, CNO, or iron nuclei. In this experiment, the network was fed a vector of 32 ADC values as input, with the maximum value at 10 or 16 time-bin respectively. Each network was trained five times. Table 4 presents the average particle recognition performance for each step and network architecture.

Table 4. The recognition efficiency (in %) of neutrinos, protons helium, CNO and iron nuclei, respectively, 12-8-3 architecture of the neural network, for 32 input time-bins in Model 2.

Network/ max time-bin position	Step 1		
	Neutrino	Proton	Background
12-8-3/10	87.3	97.6	27.3
12-8-3/16	89.5	97.2	26
	Step 2		
	Helium	CNO	Iron
12-8-3/10	74.2	9.2	42.2
12-8-3/16	74.3	9.1	42.2

Model 3 is a cascade model in which individual networks are designed to recognize specific particle types, distinguishing them from the background. The first stage detects traces generated by protons, followed sequentially by networks for neutrinos, helium nuclei, and, in the final stage, CNO and iron nuclei. We compared the performance of networks with 8-6-1, 12-8-1, and 16-12-1 architectures. Each network was trained five times. The average particle recognition performance is presented in Table 5.

© 2026 by the author(s). Distributed under a Creative Commons CC BY license.

Preprints.org (www.preprints.org) | NOT PEER-REVIEWED | Posted: 5 March 2026 doi:10.20944/preprints202603.0364.v1

Table 5. The recognition efficiency (in %) of proton, neutrino, helium, CNO and iron nuclei, respectively, for 32 input time-bins in Model 3.

Step	Particle efficiency	Network size		
		8-6-1	12-8-1	16-12-1
Step 1	Protons	89.3	93.3	91.1
	Background	87.8	89.0	88.2
Step 2	Neutrinos	85.5	83.4	84.8
	Background	46.7	46.8	48.3
Step 3	Helium	49.0	51.5	52.0
	Background	55.3	53.0	52.6
Step 4	CNO	36.1	37.3	37.2
	Iron	74.8	74.0	74.2

In the four-stage cascade model, the recognition performance for iron and CNO particles was significantly improved. However, this approach requires running four separate networks on the FPGA, each responsible for classifying particles at a specific stage. Traces that are correctly classified in the earlier stages do not need to be reprocessed in subsequent ones, which helps reduce energy consumption. Nonetheless, the overall demand for hardware resources, such as DSP blocks, remains unchanged. Although the latest FPGAs offer sufficient resources to implement such systems, they are very expensive and typically not available in standard detector configurations. Changing the architecture to 16-12-1 results in only a slight improvement in efficiency but requires a greater number of DSP blocks. Therefore, the 12-8-1 architecture appears to be the optimal choice.

In Model 4, data processing is performed in parallel by four neural networks. Each network receives the same input data vector but is responsible for classifying specific particle types. Since the recognition efficiency for protons and neutrinos is the highest (approximately 93% for protons and 83% for neutrinos) these particles are classified first, in comparison to the full background spectrum. This step has the highest priority and is handled by a dedicated network for protons and neutrinos. If particles cannot be confidently classified at this stage, a second classification step is performed, in which helium is identified against the background of CNO and iron. By excluding from background traces from protons and neutrinos, which often dominate the classification process, this step enhances the recognition efficiency for helium. This stage is assigned an intermediate priority. In the final step, which has the lowest priority, the classification between CNO and iron is carried out.

Although the recognition efficiency for individual particles is satisfactory, the system still requires four separate neural networks.

The stage 1 simulation results in Model 2 demonstrate the effectiveness of using a single network to recognize neutrinos, protons, and background signals. Model 5 improves upon Model 4 by replacing the two separate networks for recognizing neutrinos and protons with a single unified network. This network has one neuron in the output layer and produces a continuous output value: a value in the range (-1, -0.33) indicates a proton, a value in the range [-0.33, 0.33] indicates background, and a value in the range (0.33, 1) indicates a neutrino. The results from five training cycles indicate an average accuracy of 89% for neutrinos, 92% for protons, and 21% for background classification.

This model offers high particle classification capability and requires the use of three networks with a 12-8-1 architecture, which is feasible in modern FPGA systems. Based on experiments with simulation data, it can be estimated that neutrinos and protons will be classified using a priority 0 network, with accuracy levels of 91% and 94%, respectively for the best training cycle. Helium will be classified by a priority 1 network (if the priority 0 network fails to classify the particle). The accuracy of this classification is estimated at 61%. Traces generated by CNO and iron nuclei will be classified by a priority 2 network (if the previous networks fail). The classification accuracy is 39% for CNO and 73% for iron.

© 2026 by the author(s). Distributed under a Creative Commons CC BY license.

Preprints.org (www.preprints.org) | NOT PEER-REVIEWED | Posted: 5 March 2026 doi:10.20944/preprints202603.0364.v1

4. FPGA Implementation

According to the Table 6 a 4-block cascade ANN structure provides pretty good efficiency of initial particle recognition. Nevertheless, four 12-8-1 ANNs require significant amount of resources. We selected a middle size FPGA 10AS066N2F40E2SG from the Arria10 family (used also in fuzzy logic trigger [36] and LMS filter for RFI suppression [40]).

Table 6. The recognition efficiency (in %) of proton, neutrino, helium, CNO and iron nuclei, respectively, for Model 5 and 32 input time-bins in Model 4.

Network architecture	Priority	Particle	Recognition efficiency avr / best
12-8-1	0	Protons	95.0 / 95.8
		Background	82.5 / 82.5
12-8-1	0	Neutrinos	89.0 / 89.8
		Background	57.5 / 57.7
12-8-1	1	Helium	58.4 / 61.9
		CNO+Iron	46.8 / 48.9
12-8-1	2	CNO	39.0 / 39.5
		Iron	72.7 / 73.7

Table 7. The recognition efficiency (in %) of neutrinos, protons and background, respectively, for 12-8-1 architecture of the neural network, for 32 input time-bins and three levels of output.

particle	1 (%)	2 (%)	3 (%)	4 (%)	5 (%)	avr (%)
neutrino	90.4	90.1	90.3	91.2	83.2	89.0
proton	92.7	92.3	92.4	93.9	89.0	92.0
background	18.2	29.3	14.7	16.8	23.3	21.2

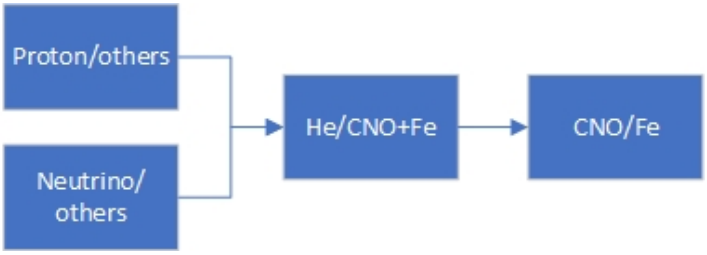

Figure 4. Data flow in 4-block configuration.

As we see from the Table 8 DSP amount has been used almost totally in 2-blocks model. The next extension have to be used without DSP blocks. Fast embedded multipliers have to be replaced by logic elements. Thus registers occupation significantly increases.

Table 8. Resources occupation for various iterations

	ALMs	Regs	Memory bits	DSPs	Slow 100 MHz	Slow 0 MHz
1-block	12 298 (5%)	42 614	11 599 872	732 (43%)	149.19	164.39
2-blocks	24 309 (10%)	84 853	18 481 152	1464 (87%)	147.84	163.67
3-blocks	43 119 (17%)	143 301	25 362 432	1467 (87%)	156.2	173.34

© 2026 by the author(s). Distributed under a Creative Commons CC BY license.

Preprints.org (www.preprints.org) | NOT PEER-REVIEWED | Posted: 5 March 2026 doi:10.20944/preprints202603.0364.v1

Flow Summary

<<Filter>>

Flow Status	Successful - Fri Feb 20 11:06:43 2026
Quartus Prime Version	22.1std.0 Build 915 10/25/2022 SC Standard Edition
Revision Name	ANN07_32x10_12x8x1_16384_3channels_4steps_2xDSP_2xnoDSP
Top-level Entity Name	ANN07_32x10_12x8x1_16384_3channels_4steps_2xDSP_2xnoDSP
Family	Arria 10
Device	10AS066N2F40E2SG
Timing Models	Final
Logic utilization (in ALMs)	61,591 / 251,680 (24 %)
Total registers	201194
Total pins	205 / 812 (25 %)
Total virtual pins	0
Total block memory bits	27,525,120 / 43,642,880 (63 %)
Total DSP Blocks	1,488 / 1,687 (88 %)
Total HSSI RX channels	0 / 48 (0 %)
Total HSSI TX channels	0 / 48 (0 %)
Total PLLs	0 / 96 (0 %)

Slow 900mV 100C Model Fmax Summary

<<Filter>>

	Fmax	Restricted Fmax	Clock Name
1	188.15 MHz	188.15 MHz	Clk

Slow 900mV 0C Model Fmax Summary

<<Filter>>

	Fmax	Restricted Fmax	Clock Name
1	215.47 MHz	215.47 MHz	Clk

Figure 5. Summary for Quartus project compilation.

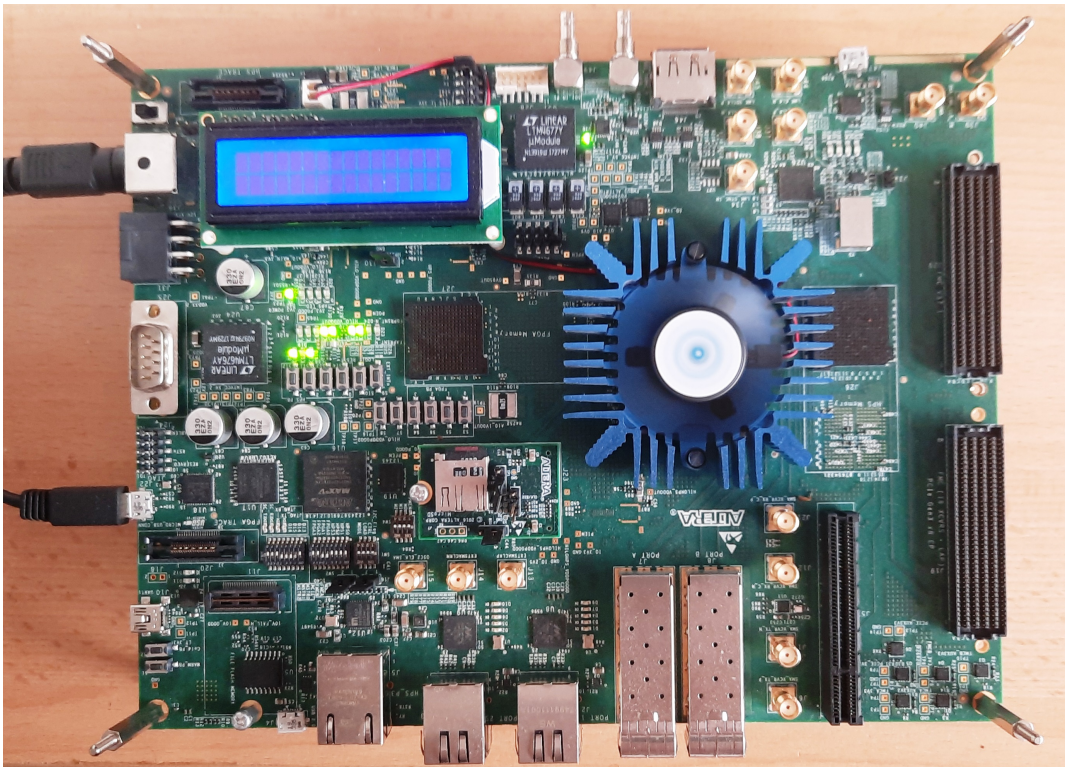

Figure 6. Intel Arria10 SX SoC Development Kit used for hardware verification of the neural network algorithm.

The final project with 4-steps configuration uses 24% of ALMs and 74% of internal memory for ADC delay lines (ca 4 kB) and tansig coefficients. The safety margin is very wide for 120 MHz sampling ADC frequency.

© 2026 by the author(s). Distributed under a Creative Commons CC BY license.

Preprints.org (www.preprints.org) | NOT PEER-REVIEWED | Posted: 5 March 2026 doi:10.20944/preprints202603.0364.v1

5. Models Testing on Real Data Recorded at Auger

Since 2015 the entire surface detector electronics is being updated. The old Unified Boards (UB) with plugged in Front End Boards (FEB), equipped with Altera Cyclone FPGAs and 10-bit 40 MHz ADCs, have been replaced by Updated Unified Boards (UUB) with Zynq7020 (Xilinx) FPGAs and integrated with the board 120 MHz 12-bit ADCs. UB registered 10-bit event profiles with 768 time-bins, while UUB register 12-bit profiles of 2048 time-bins [41].

5.1. Undershoot

Average pedestal was on a level of 200 ADC_units. This pedestal was subtracted from ADC data for MATLAB processing. However, in real experimental Auger data we observe very often undershoots (Figure 7), where a signal momentarily dips below its target or desired level before settling to its final value. Undershoots can be caused by various factors, including reflections within transmission lines, the interaction of multiple signals, and the behavior of components in the circuit, e.g. AC-coupling.

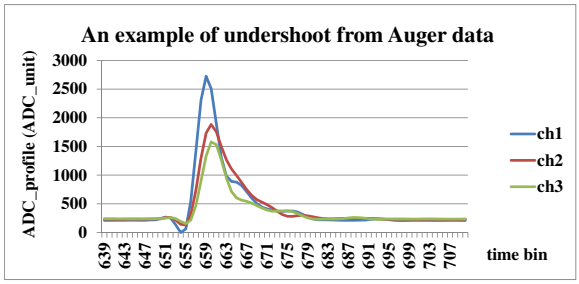

Figure 7. An example of undershoot from experimental Auger data.

Undershoots dramatically get worse MATLAB estimations. The Pierre Auger Observatory did not register any neutrino-induced event since the beginning of operation. This maybe due to either extremely low neutrino flux or very low trigger efficiency for neutrino-induced showers. Therefore the graph showing a level of about 24% of detected neutrinos is unreliable (Figure 8).

A choice of minimum subtraction (Figure 8A) reduces false neutrino recognition on the level of magnitude. However, a level of ∼2.8 % is still rather high. Although a level of ∼3 % is not dangerous for the DAQ, it is still far from potential saturation of the transmission channel due too high trigger rate. Nevertheless, this level of the false recognition could be still decreased by more advanced neural network (Figure 8B).

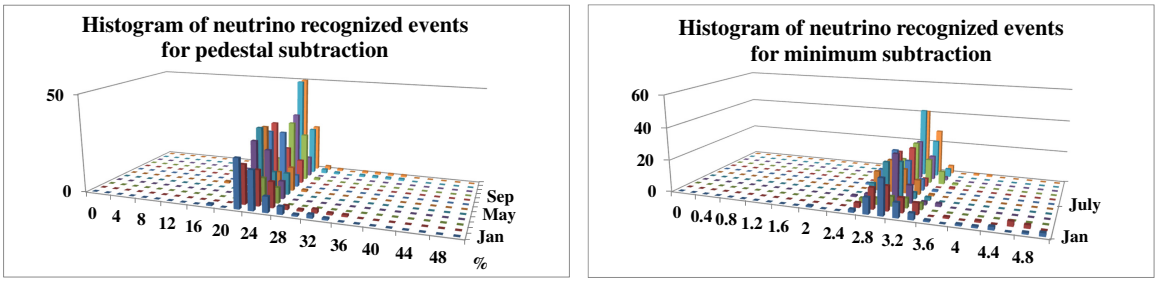

Figure 8. Histograms of percent contribution of recognized neutrino-induced events after the pedestal subtraction from ADC data (left plot) and after the minimum subtraction from ADC data (right plot).

5.2. Triggers

The Auger surface detector is triggered by 4 parallel triggers:

1. THR - Single bin Threshold trigger
2. ToT - Time over Threshold trigger
3. ToTd - Time over Threshold deconvoluted

© 2026 by the author(s). Distributed under a Creative Commons CC BY license.

Preprints.org (www.preprints.org) | NOT PEER-REVIEWED | Posted: 5 March 2026 doi:10.20944/preprints202603.0364.v1

4. MoPS - Multiplicity of Positive Steps

The main trigger is the shower trigger that results in the recording of 768 samples (19.2 μs) of the six FADCs. It has two levels of selection. The first level, called T1, has 2 independent modes. The first one is a simple threshold trigger (THR) requiring the coincidence of all three PMTs being above 1.75 I_{VEM}. This trigger is used to select large signals that are not necessarily spread in time. It is particularly effective for the detection of very inclined showers that have penetrated through a large atmospheric depth and are consequently dominantly muonic. The threshold has been adjusted to reduce the rate of atmospheric muon triggers from about 3 kHz to 100Hz. The second T1 mode is a time-over-threshold trigger (ToT)requiring that at least 13 bins with in a 3 μs window (120 samples) exceed a threshold of 0.2 I_{VEM} in coincidence for two out of the three PMTs. The ToT trigger selects sequences of small signals spread in time, and is thus efficient for the detection of vertical events, and more specifically for stations near the core of low- energy showers, or stations far from the core of high-energy showers. The rate of the ToT trigger depends on the shape of the muon pulse in the tank and averages to 1.2 Hz with a rather large spread (about 1Hz rms). The second trigger level, called T2, is applied to decrease the global rate of the T1 trigger down to about 23 Hz. While all T1-ToT triggers are promoted to T2-ToT, only T1-TH triggers passing a single threshold of 3.2 I_{VEM} in coincidence for the three PMTs will pass this second level and become T2-TH. All T2s send their time-stamp to CDAS for the global trigger (T3) determination [42].

The additional trigger algorithms, Time-over-Threshold de-convoluted (ToTd) and Multiplicity of Positive Steps (MoPS), were designed to be insensitive to atmospheric muons by enabling the detection of extended low-amplitude signals (lower than those sampled by the standard ToT), such as those created by the electromagnetic component in low-energy showers or at the outskirts of higher-energy ones. By extending the sensitivity of individual stations, the additional triggers increase the number of triggered stations and allow events with lower overall signal to be recorded, with the goal of lowering the effective energy threshold of the SD, in particular for electromagnetic primaries, i.e., photons and neutrinos.

The ToTd trigger is based on the characteristic decay time of Cherenkov light inside the water tank. The recorded waveform is first de-convoluted to suppress the exponential tail associated with the light decay, after which a time-over-threshold condition is ap- plied. This procedure reduces the probability that muon-like signals satisfy the trigger, while preserving signals with a significant electromagnetic component. The MoPS trig- ger identifies signals by counting the number of consecutive increases in the digitized waveform amplitude within a sliding time window. This method is independent of the absolute VEM calibration and is sensitive to small, non-smooth signals produced by multiple electromagnetic particles arriving over an extended period of time. As a result, MoPS efficiently selects electromagnetic shower signals while remaining insensitive to isolated muon pulses. External (Ext) and Random (Rnd) triggers are also used for a diagnostics.

Table 9. Number of events for various triggers for entire 2024 year.

THR	ToT	ToTd	MoPS	Ext	Rnd	7	8	other
9 619 815	1 778 208	6450	319 163	25	2616	8	1 231 940	16 984

5.3. Particles Identification on ADC Profiles

Profiles for identification are built from 32 ADC consecutive sa mples. So, events triggered by THR correspond the best as patterns. The Table 10 summarizes contributions of recognized particles in THR trigger for 2024. The other triggers are temporarily neglected. Relatively simple neural 12-8-5 network was used (taught on CORSIKA and OffLine simulations).

According our expectations the main contribution comes from protons. Neutrinos are represented at a level 1.6 %. This is probably too big value, as up to now the Auger Observatory did not register neutrino-induced event. Helium and CNO fraction are represented in reasonable values. The iron

© 2026 by the author(s). Distributed under a Creative Commons CC BY license.

Preprints.org (www.preprints.org) | NOT PEER-REVIEWED | Posted: 5 March 2026 doi:10.20944/preprints202603.0364.v1

is rather not recognized. We made 5 MATLAB simulations for 200 epochs each. Due to a random algorithm values in each simulation differ each other and even iron appears in residual form.

We checked the same Auger data with much more sophisticated neural network : 32-24-16-12-8-5 (not especially for real FPGA implementation due to a huge resources occupancy) (Table 10).

Table 10. Contribution of recognized initial particles in Auger traces from 2024 for only THR trigger. 3-layer (12-8-5) and 6-layer (32-24-16-12-8-5) networks were used. Pedestal was subtracted. In case of undershoot, negative values in profiles were put arbitrarily zeros. Profiles with saturation were neglected.

Only THR trigger, no saturated events						
12-8-5	1^{st} sim	2^{nd} sim	3^{rd} sim	4^{th} sim	5^{th} sim	average
ν	1.61 %	1.61 %	1.65 %	2.63 %	0.80 %	1.66 %
p	89.43 %	89.43 %	86.32 %	86.76 %	91.24 %	88.64 %
He	5.98 %	5.98 %	5.85 %	5.85 %	0.81 %	4.96 %
CNO	2.98 %	2.98 %	4.76 %	4.76 %	7.14 %	4.74 %
Fe	0.00 %	0.00 %	0.00 %	0.00 %	2.9E-4 %	5.8E-5 %
32-24-16-12-8-5	1^{st} sim	2^{nd} sim	3^{rd} sim	4^{th} sim	5^{th} sim	average
ν	0.39 %	0.25 %	0.36 %	0.55 %	0.18 %	0.34 %
p	86.29 %	81.01 %	80.20 %	81.76 %	76.97 %	81.25 %
He	1.91 %	6.95 %	8.11 %	4.65 %	1.17 %	4.56 %
CNO	11.40 %	11.51 %	11.13 %	12.92 %	21.64 %	13.72 %
Fe	0.0052 %	0.27 %	0.20 %	0.13 %	0.04 %	0.13 %

Table 11. Contribution of recognized initial particles in Auger traces from 2024 for only THR trigger, but with also saturated events. 3-layer (12-8-5) and 6-layer (32-24-16-12-8-5) networks were used. Pedestal was subtracted. In case of undershoot, negative values in profiles were put arbitrarily zeros.

Only THR trigger, but with saturated events						
12-8-5	1^{st} sim	2^{nd} sim	3^{rd} sim	4^{th} sim	5^{th} sim	average
ν	3.07 %	3.07 %	1.56 %	3.49 %	2.07 %	2.65 %
p	92.80 %	92.80 %	93.37 %	89.70 %	94.95 %	92.72 %
He	2.48 %	2.48 %	2.68 %	2.54 %	0.38 %	2.11 %
CNO	1.63 %	1.63 %	2.38 %	4.26 %	2.59 %	2.50 %
Fe	0.02 %	0.02 %	0.002 %	0.007 %	0.011 %	0.013 %
32-24-16-12-8-5	1^{st} sim	2^{nd} sim	3^{rd} sim	4^{th} sim	5^{th} sim	average
ν	0.59 %	0.51 %	0.56 %	0.71 %	0.51 %	0.57 %
p	92.36 %	90.91 %	91.89 %	90.75 %	77.34 %	88.65 %
He	0.46 %	2.01 %	1.50 %	0.97 %	0.45 %	1.08 %
CNO	6.24 %	6.28 %	5.23 %	7.19 %	21.44 %	9.27 %
Fe	0.35 %	0.29 %	0.83 %	0.37 %	0.26 %	0.42 %

Table 12 shows simulation results for 3-, 4-, 5- and 6-layer networks. More complicated network (beginning from 4-layer) recognizes less neutrino and proton events, , simulteneously increases recognition for He, CNO and Fe. We can notice that differences betwwen 4- and 5-layer networks are rather ststistical. Only 6-layer network shows a statistical difference from the previous ones. The 6-layer network is too sophisticated and resource consuming for the FPGA implementation. Even 5-layer is problematic due to a lack of DSP fast multipliers. A part of multipliers have to be implemented as a simple logic, which dramatically increase a use of ALMs. The reasonable compromise seems to be an implementation of 4-layer network with not too big neutrino fraction and reasonable contributions of the rest of particles: p, He, CNO and Fe (Figure 9).

Both networks provide very wide safety margin for 120 MHz ADC sampling. Even for 4-layer network all multipliers are implemented in DSP blocks. Resources occupancy is at a level of 8 %, memory occupancy at a level of 22 %. Arria10 FPGA seems to be pretty good for our design. Generally, it seems that results from Tables 10 - 12 are consistent with data from Figure 2.

© 2026 by the author(s). Distributed under a Creative Commons CC BY license.

Preprints.org (www.preprints.org) | NOT PEER-REVIEWED | Posted: 5 March 2026 doi:10.20944/preprints202603.0364.v1

Table 12. Contribution of recognized initial particles in Auger traces from 2024 for all triggers. from 3-layer (12-8-5) up to 6-layer (32-24-16-12-8-5) networks were used. Pedestal was subtracted. In case of undershoot, negative values in profiles were put arbitrarily zeros.

All used triggers, also with saturated events						
12-8-5	1^{st} sim	2^{nd} sim	3^{rd} sim	4^{th} sim	5^{th} sim	average
ν	1.22 %	1.22 %	1.22 %	2.16 %	1.23 %	1.41 %
p	91.53 %	91.53 %	81.20 %	89.08 %	95.25 %	89.72 %
He	2.92 %	2.92 %	0.62 %	2.76 %	0.41 %	1.93 %
CNO	2.54 %	2.54 %	16.68 %	3.17 %	2.81 %	5.55 %
Fe	1.78 %	1.78 %	0.28 %	2.83 %	0.29 %	1.40 %
16-12-8-5	1^{st} sim	2^{nd} sim	3^{rd} sim	4^{th} sim	5^{th} sim	average
ν	0.57 %	2.30 %	0.51 %	0.52 %	0.54 %	0.89 %
p	90.42 %	79.46 %	74.48 %	76.36 %	92.49 %	82.64 %
He	0.13 %	1.59 %	2.36 %	2.49 %	5.25 %	2.36 %
CNO	8.62 %	5.89 %	21.50 %	18.14 %	1.54 %	11.14 %
Fe	0.26 %	10.75 %	1.16 %	2.49 %	0.18 %	2.97 %
24-16-12-8-5	1^{st} sim	2^{nd} sim	3^{rd} sim	4^{th} sim	5^{th} sim	average
ν	0.34 %	0.35 %	3.54 %	0.36 %	3.63 %	1.64 %
p	80.34 %	80.32 %	76.11 %	77.40 %	81.19 %	79.08 %
He	0.69 %	0.70 %	14.44 %	0.67 %	1.28 %	3.56 %
CNO	18.59 %	18.58 %	5.72 %	21.50 %	13.70 %	15.62 %
Fe	0.03 %	0.04 %	0.19 %	0.06 %	0.21 %	0.11 %
32-24-16-12-8-5	1^{st} sim	2^{nd} sim	3^{rd} sim	4^{th} sim	5^{th} sim	average
ν	0.44 %	0.37 %	0.30 %	0.53 %	0.34 %	0.40 %
p	69.13 %	79.63 %	79.13 %	69.43 %	70.90 %	73.64 %
He	2.15 %	2.61 %	5.73 %	21.41 %	0.28 %	6.44 %
CNO	28.12 %	17.19 %	14.55 %	8.49 %	28.40 %	19.35 %
Fe	0.18 %	0.21 %	0.29 %	0.08 %	0.08 %	0.17 %

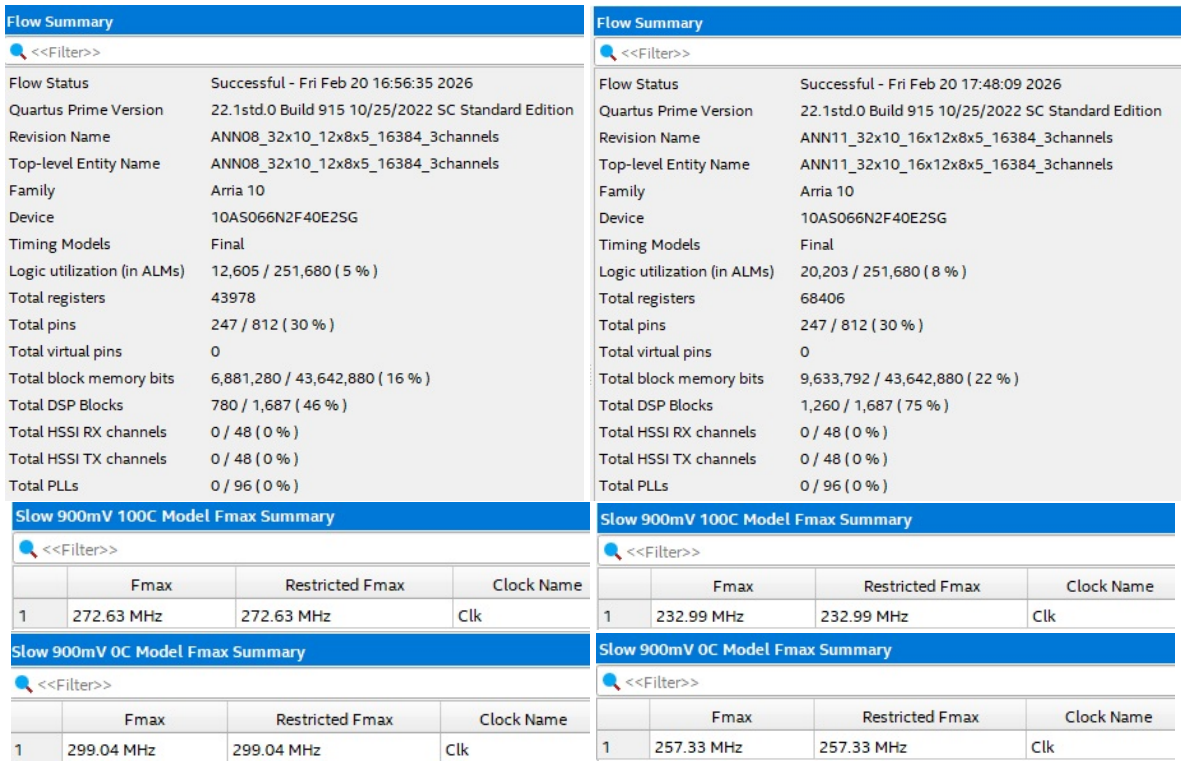

Figure 9. Resources occupancy for 3-layer (12-8-5) and 4-layer (16-12-8-5) networks as well as F_{max} for Slow models for 100 °C and 0 °C for 3-layer (left) and 4-layer (right) designs.

© 2026 by the author(s). Distributed under a Creative Commons CC BY license.

Preprints.org (www.preprints.org) | NOT PEER-REVIEWED | Posted: 5 March 2026 doi:10.20944/preprints202603.0364.v1

The network 32-24-16-12-8-5 recognizes iron better and the contribution of neutrino is lower, as we expected. Some surprise is a relatively strong contribution of CNO fraction.

Taking into account saturated events increases a contribution of neutrinos, protons and also irons, decreasing simultaneously He and CNO fractions. In comparison to data from Table 10 the contribution of iron is bigger at a cost of CNO fraction. Neutrinos and Helium remain at a similar level.

6. Conclusions

The trigger based on neural networks provides surprising extremely high recognition efficiency of neutrino/proton patterns. Patterns are almost perfectly recognized independently of zenith angle, energy and the slant depth. Extremely high recognition efficiency provided originally in MATLAB has been fully confirmed on hardware platforms Arria10. Triggers are working stable by 125 MHz global clock with a sufficient safety margin.

In our opinion the FPGA neural network trigger could help in online identification primary particles of UHECRs in Auger surface detectors.

Acknowledgments: The author would like to thank Colleagues from Karlsruhe Institute of Technology for the access to CORSIKA and OffLine simulation software as well as Intel Corporation for licenses for Quartus Standard and Quartus Pro compilers made available free of charge for research.

References

1. M. Nagano, A.A. Watson, "Observations and implications of the ultrahigh-energy cosmic rays", *Rev. Mod. Phys.* 72 (2000) 689.
2. B.R. Dawson, M. Fukushima, P. Sokolsky, "Past, present, and future of UHECR observations", *Prog. Theor. Exp. Phys.* 12 (2017) A101.
3. S. Mollerach and E. Roulet, "Progress in high-energy cosmic ray physics", *Prog. Part. Nucl. Phys.* 98 (2018) 85.
4. A.M. Hillas, "The origin of ultra-high-energy cosmic rays", *Annual Review of Astronomy and Astrophysics*, Vol. 22, pp. 425-444, 1984.
5. D.F. Torres, L. Anchordoqui, "Astrophysical origins of ultrahigh energy cosmic rays", *Reports on Progress in Physics*, vol. 67, no. 9, pp. 1663–1730, July 2004.
6. A. Aab (The Pierre Auger Collaboration), "The Pierre Auger Cosmic Ray Observatory", *Nucl. Instrum. Meth.*, vol. A798, pp. 172-213, 2015.
7. The Pierre Auger collaboration, J. Abraham et al., "Measurement of the energy spectrum of cosmic rays above 10^{18} eV using the Pierre Auger Observatory", *Phys. Lett. B* 685 (2010) 239 [arXiv:1002.1975] [SPIRES].
8. HiRes collaboration, R.U. Abbasi et al., "Observation of the GZK cutoff by the HiRes experiment", *Phys. Rev. Lett.* 100 (2008) 101101 [astro-ph/0703099] [SPIRES].
9. K. Greisen, "End to the cosmic ray spectrum?", *Phys. Rev. Lett.* 16 (1966) 748 [SPIRES].
10. G.T. Zatsepin and V.A. Kuz'min, "Upper limit of the spectrum of cosmic rays", *JETP Lett. 4* (1966) 78 [Pisma Zh. Eksp. Teor. Fiz. 4 (1966) 114] [SPIRES].
11. D. Harari, S. Mollerach and E. Roulet, "On the ultra-high energy cosmic ray horizon", *JCAP 11* (2006) 012 [astro-ph/0609294] [SPIRES].
12. A.V. Olinto, D. Allard, E. Armengaud and A. Kravtsov, "Horizons and anisotropies of ultra-high energy cosmic rays", *in Proceedings of the 30th International Cosmic Ray Conference (ICRC) 4* (2008) 527.
13. The Pierre Auger collaboration, J. Abraham et al., "Correlation of the highest energy cosmic rays with nearby extra-galactic objects", *Science 318* (2007) 938 [arXiv:0711.2256] [SPIRES].
14. The Pierre Auger collaboration, J. Abraham et al., "Correlation of the highest-energy cosmic rays with the positions of nearby active galactic nuclei", *Astropart. Phys.* 29 (2008) 188 [Erratum ibid. 30 (2008) 45] [arXiv:0712.2843] [SPIRES].
15. The Pierre Auger collaboration, P. Abreu et al., "Update on the correlation of the highest energy cosmic rays with nearby extragalactic matter", *Astropart. Phys.* 34 (2010) 314 [arXiv:1009.1855] [SPIRES].
16. D. Allard, A. Olinto, and E. Parizot, "Signatures of the extragalactic cosmic-ray source composition from spectrum and shower depth measurements", *Astron. Astrophys.* 473, 59 (2007).

© 2026 by the author(s). Distributed under a Creative Commons CC BY license.

Preprints.org (www.preprints.org) | NOT PEER-REVIEWED | Posted: 5 March 2026 doi:10.20944/preprints202603.0364.v1

17. R. Aloisio, V. Berezinsky, and P. Blasi, "Ultra high energy cosmic rays: implications of Auger data for source spectra and chemical composition", *J. Cosmol. Astropart. Phys.* 10 (2014) 020.
18. A. M. Taylor, M. Ahlers, and D. Hooper, "Indications of negative evolution for the sources of the highest energy cosmic rays", *Phys. Rev. D* 92, 063011 (2015).
19. Pierre Auger Collaboration, "Combined fit of spectrum and composition data as measured by the Pierre Auger Observatory", *J. Cosmol. Astropart. Phys.* 04 (2017) 038.
20. Pierre Auger Collaboration, "Depth of maximum of air-shower profiles at the Pierre Auger Observatory. I. Measurements at energies above $10^{17.8}$ eV", *Phys. Rev. D* 90, 122005 (2014).
21. Pierre Auger Collaboration, "Depth of maximum of air-shower profiles at the Pierre Auger Observatory. II. Composition implications", *Phys. Rev. D* 90, 122006 (2014).
22. A. Yushkov (Pierre Auger Collaboration), *Proc. Sci., ICRC2019* (2019) 482, https://pos.sissa.it/358/482/pdf.
23. T. Pierog, I. Karpenko, J. M. Katzy, E. Yatsenko, and K. Werner, "EPOS LHC: Test of collective hadronization with data measured at the CERN Large Hadron Collider", *Phys. Rev. C* 92, 034906 (2015).
24. Pierre Auger Collaboration, "Features of the Energy Spectrum of Cosmic Rays above 2.5×10^{18} eV Using the Pierre Auger Observatory", *Phys. Rev. Lett. 125, 121106* (2020)
25. CORSIKA an Air Shower Simulation Program [Online]. Available: https://web.ikp.kit.edu/corsika/.
26. S. Argiro et al., "The offline software framework of the Pierre Auger Observatory", *Nucl. Instrum. Methods, A580*, pp. 1485–1496, 2007.
27. Z. Szadkowski, K. Pytel, "Proposal of the FPGA neural network trigger for the surface detector of the Pierre Auger Observatory to recognize neutrino-induced showers", submitted to *Journal of Supercomputing*
28. A.d.Supanitsky, "Determination of the Cosmic-Ray Chemical Composition: Open Issues and Prospects", *Galaxies 2022, 10, 75.* https://doi.org/10.3390/galaxies10030075
29. Zurada, J.M. (1992) Introduction to Artificial Neural Systems. West Publishing Company, St. Paul.
30. Aggarwal, Charu C., (2023), Neural Networks and Deep Learning. A Textbook. Springer.
31. Graupe Daniel, (2007), Principles of Artificial Neural Networks, World Scientific Pub Co Inc.
32. Bishop Christopher M., (1995), Neural Networks for Pattern Recognition. UK Clarendon Press, Oxford.
33. Z.Szadkowski, D.Głas, K.Pytel, M.Wiedeński, "Optimization of an FPGA Trigger Based on an Artificial Neural Network for the Detection of Neutrino-Induced Air Showers", *IEEE Trans. Nucl. Science,* vol. 64 pp. 1271-1281, 2017.
34. online: https://www.terasic.com.tw/
35. online: https://en.wikipedia.org/wiki/ModelSim
36. Z. Szadkowski, K. Pytel, "Trigger Based on Fuzzy Logic for the detection of Neutrino-Induced Extensive Air Showers in Water-Cherenkov Detectors", *European Phys. Journal Plus*, 138:809, 2023, https://doi.org/10.1140/epjp/s13360-023-04411-5
37. Z. Szadkowski, K.Pytel, "Proposal of the Fuzzy Trigger for the Surface Detector of the Pierre Auger Observatory", *IEEE Trans. Nucl. Science*, vol. 71, no.6, pp. 1281-1291, 2024.
38. Z. Szadkowski, "Front-End Board with Cyclone V as a Test High-Resolution Platform for the Auger_Beyond_2015 Front End Electronics", *IEEE Trans. Nucl. Science*, vol. 62, no.3, pp. 985-992, 2015.
39. Z. Szadkowski, "Tests of High-Resolution Front-End Electronics for Water-Cherenkov Air Shower Detectors Equipped With Cyclone V on the Pierre Auger Test Array", *IEEE Trans. Nucl. Science*, vol. 65, no.2, pp. 805-813, 2018.
40. Z. Szadkowski, "Multistage FPGA Least Mean Squares Filters Suppressing Multiple Narrowband Radio-Frequency Interferences in the Radio Detection of Cosmic Rays", *IEEE Trans. Nucl. Science*, vol. 70, no. 5, 2023
41. A. Aab (The Pierre Auger Collaboration), "The Pierre Auger Observatory open data", Jan 24 2025, *European Phys. Journal C*, 85 (1)
42. J.Abraham, et.al., "Trigger and aperture of the surface detector array of the Pierre Auger Observatory", *Nuclear Instruments and Methods in Physics Research*, A613(2010)29. http://dx.doi.org/10.1016/j.nima.2009.11.018 (arXiv:1111.6764).

Disclaimer/Publisher's Note: The statements, opinions and data contained in all publications are solely those of the individual author(s) and contributor(s) and not of MDPI and/or the editor(s). MDPI and/or the editor(s) disclaim responsibility for any injury to people or property resulting from any ideas, methods, instructions or products referred to in the content.

© 2026 by the author(s). Distributed under a Creative Commons CC BY license.